ELSEVIER

Ceramics International 27 (2001) 63–71

CERAMICS INTERNATIONAL

www.elsevier.com/locate/ceramint

Population balance model for solid state sintering II. Grain growth

S. Sivakumar [a], Manjunath Subbanna [a], Satyam S. Sahay [a], Vijay Ramakrishnan [a], P.C. Kapur [a], Pradip [a,*], S.G. Malghan [b]

[a] *Tata Research Development and Design Centre, Plot # 54 B, Hadapsar Industrial Estate, Pune 411 013, India*
[b] *National Institute of Standards and Technology, 100 Bureau Drive, Gaithersburg, MD 20899-0001, USA*

Received 14 January 2000; received in revised form 8 February 2000; accepted 2 March 2000

Abstract

A novel population balance model based on size interval-by-size interval marching algorithm has been developed for the transient grain growth kinetics during solid state sintering. This model incorporates the coupled phenomena of densification and grain growth and exhibits reasonable capability of predicting the temporal evolution of grain size distribution for a given initial grain size distribution and time-temperature sintering cycle. In this, part II of our work, we present the coupled governing equation for sintering kinetics. We employ a size interval-by-size interval marching algorithm for the solution of the resulting population balance equation and validation of the model against experimental data for zirconia compacts sintered at 1400, 1500 and 1600°C for different times. In addition, the model has been successfully tested against published experimental data on sintering of alumina compacts.

Keywords: A. Grain growth; A. Sintering; B. Grain size; B. Microstructure-final

1. Introduction

Crystalline and nano-crystalline powders are consolidated and sintered to obtain dense polycrystalline products in the manufacturing of engineering ceramics. The mechanical properties of the engineering ceramics are strongly dependent on the microstructural features such as grain size, shape and size distribution, besides total porosity and pore size distribution [1,2]. Even though trial and error based processing routes are widely employed in practice, in general, the sintering process is difficult to control by such empirical strategies. During the sintering process, massive microstructural changes occur as a result of a complex interplay of various material transport mechanisms, necessitating a greater understanding of the process [3–5]. Realistic, but tractable, mathematical models can contribute greatly to our understanding of the process as well as controlling and optimizing it.

The existing theories of grain growth are mostly based on average grain size leading to power law type kinetic expressions [6–8]. Others are based on an assumption of a specific distribution function — lognormal, for example [9,10] — or a steady-state distribution, which may or may not conform to one of the standard statistical distributions [11–14]. It is evident that a single parameter description of grain size distribution is simply too abbreviated for any meaningful predictive simulation and process optimization. Imposition of an ad hoc distribution is not only misleading, more importantly, it completely discounts the possibility of the template effect of the precursor powder on the evolving grain size spectrum. The stationary or self-similar distribution, in particular, implies that the effect of the initial powder or grain size distribution is totally obliterated or smoothened out after a sufficiently long sintering time at a sufficiently high firing temperature, which is generally not observed in practice [15,16]. On the other hand, computer simulations by present authors and others show [15–18] that the stationary state is attained, if at all, only after a long time, more so, if the initial distribution has a broader dispersion in size than the final steady or near steady

* Corresponding author. Fax: +91-20-6810921.
E-mail address: pradip@pune.tcs.co.in (Pradip).

0272-8842/01/$20.00
PII: S0272-8842(00)00042-0

state distribution. In order to avoid abnormal/secondary grain growth, ceramic systems in general are unlikely to be driven to a true steady state. In other words, the effect of the starting powder distribution on grain size evolution and pore shrinkage is not insignificant [11,19–22] and, as such, it may not be realistic to ignore it in sintering analysis.

A comprehensive detailed population balance based model of sintering should address grain growth and pore shrinkage together, as proposed by Pradip [23]. The coupled equations for grain growth and pore shrinkage then must be solved simultaneously in order to predict the evolution of microstructure during sintering. In Part I [24] of this series, a model for pore shrinkage and densification was presented. In this part, a methodology for modeling the grain growth kinetics — coupled to the rate of densification or shrinkage of pores — during the intermediate stage of sintering is reported. A formal population balance approach is employed to predict the temporal evolution of the grain size distribution in the intermediate/final stage for a given initial grain size distribution and time-temperature sintering cycle. The resulting model equations are solved in the transitory (non-stationary) regime with a specially devised size interval-by-size interval marching algorithm.

2. Population balance approach to kinetics of grain growth

The general phenomenological approach based on a formal population balance on the growing/shrinking particulate entities that are not necessarily ceramic grains is well established [25,26]. Assuming a spatially homogeneous ceramic body and assuming coalescence free and convectionless batch process [23], the continuity equation for the trajectory of the grain size distribution is given by [15,23,27,28]:

$$\frac{\partial H(r,t)}{\partial t}+\frac{\partial}{\partial r}(v_r H(r,t))=0 \tag{1}$$

where $H(r,t)$ is the number density function of the grain of radius r at sintering time t. The generalized velocity function v_r for the rate of growth/decay of a grain can be described by [29]:

$$\frac{\mathrm{d}r}{\mathrm{d}t}=i_r=\frac{C_\mathrm{G}}{[1-\rho(t)]^{\alpha}r^{n}}\left(\frac{1}{r_\mathrm{c}}-\frac{1}{r}\right) \tag{2}$$

where n and α are model parameters, ρ(t) is relative density, and $r_\mathrm{c}(t)$ is the instantaneous critical radius, defined as the radius of a grain which neither shrinks nor grows at any instant of time. C_G is a temperature dependent rate constant, given by the following Arrhenius form:

$$C_\mathrm{G}=B\exp\left(-\frac{Q_\mathrm{G}}{RT}\right) \tag{3}$$

The parameter Q_G is generally referred to as the overall activation energy for grain growth. These sintering parameters are often related to diffusivity and surface free energy of the solid, and the various material transport mechanisms (e.g. lattice, surface and grain boundary diffusions, vapor transport etc) during the grain growth. Combining Eqs. (1) and (2) yields:

$$\frac{\partial H}{\partial t}+\frac{\partial}{\partial r}\left(\frac{C_\mathrm{G}H}{[1-\rho(t)]^{\alpha}r^{n}}\left(\frac{1}{r_\mathrm{c}}-\frac{1}{r}\right)\right)=0 \tag{4}$$

The term containing relative density ρ in the equation accounts for the effect of densification on grain growth. The relative density can be expressed as follows:

$$\rho(t)=\frac{1}{1+\dfrac{V(t)}{V(0)}\left[\dfrac{1}{\rho(0)}-1\right]} \tag{5}$$

$V(t)$, the total pore volume at time t can be computed by the densification model [Eq. (10)] given in Part I [24].

A general closed form analytical solution to the Eq. (4), is not possible. Tomandl [15], Venzl [17] and more recently Fang [32] have attempted a numerical solution of similar equations of sintering and grain growth. Tomandl's paper does not include sufficient information on the initial size distribution, special interpolation technique employed for introducing new grid points etc., to carry out an independent validation of his method. However, he did report problems of numerical instability in his method for some class of initial distributions. Venzl's work is restricted to Ostwald ripening in supersaturated solutions for a limited number of distributions only. Fang sought to solve the equation of continuity by the finite difference technique. Apart from heavy computational load inherent in the scheme, he required frequent checks and manipulations to conserve the solid volume. This paper presents a relatively straightforward and demonstrably accurate numerical size interval-by-size interval marching algorithm for solving the governing grain growth equation. The results are compared [16] with steady-state asymptotic solutions, valid for long time only, that are available for simplified velocity functions without the density term in Eq. (2) [15,30,31].

3. Solution methodology

The size interval-by-size interval marching algorithm for solving the governing equations is briefly described here. The algorithm was utilised in solving an earlier model [16] that had a simplified velocity function. The present demonstration is more general as it incorporates

the coupled phenomenon of densification and grain growth.The marching algorithm exploits the fact that in a physically realizable deterministic process the relative ordering of grains by size remains unchanged as they grow and or shrink in the absence of coalescence and breakage phenomena. This simply means that no grain can "jump the queue" in the sample domain. As a consequence, when a grain of size r_1 at time t_1 changes over to r_2 at time t_2, then the following equality must hold:

$$R(r_1, t_1) = R(r_2, t_2) \tag{6}$$

where R is the cumulative larger distribution function given by:

$$R(r, t) = \frac{\int_r^\infty H(r, t)\mathrm{d}r}{\int_0^\infty H(r, t)\mathrm{d}r} \tag{7}$$

Moreover, r_1 and r_2 are related by the velocity function in Eq. (2). Incidentally, this property was employed by DeHoff [33] also in his grain path envelope analysis.

For implementing the algorithm, the initial cumulative larger size distribution $R(r,t=0)$ is discretized into N size intervals, where N is of the order of 1000 or more.

The j-th interval is bounded by $r_j(t=0) < r < r_{j+1}(t=0)$; $j=0,1,..$ The moments in terms of cumulative distribution are given as:

$$M_0(t) = R(0, t) \tag{8}$$

and

$$M_k(t) = k\int_0^\infty R(r, t)r^{k-1}\mathrm{d}r \quad k = 1, 2, .. \tag{9}$$

Using Eq. 4 and the volume conservation property of the third moment, M_3(t), the following expression for the critical radius r_c is obtained:

$$r_c = \frac{M_{2-n}}{M_{1-n}} \tag{10}$$

A cubic spline interpolation in conjunction with a numerical integration scheme is convenient for computing the moments in Eq. (9). In the first iteration, starting from time $t=0$, the velocity function in Eq. (2) is integrated and solved for Δt, the time required to dissolve all grains in the smallest interval $0 < r < r_1(0)$, that is, for all grains of maximum size $r_1(0)$ to disappear completely. Eq. (2) is then integrated over the time interval Δt for all sizes $r_j(0)$ other than the size $r_1(0)$. A new size list of $r_j(\Delta t)$ is thus generated in which the first size interval is bounded by zeroes (empty or null interval). Because of the queue constraint, the number of grains remains unchanged in all other intervals. The third moment of the resulting size distribution is checked to ensure that the total grain volume is conserved. The second iteration is initiated by calculating r_c and Δt once more, the latter by dissolving all grains in the second interval. Following this, the steps enumerated above are repeated. In this manner, the time interval for integration is chosen adaptively so as to dissolve all the grains in the smallest non-empty interval, after each iteration.

In the absence of analytical solutions of the grain growth continuity equation in the transitory regime, the marching algorithm can be checked only indirectly by verifying the conservation of grain volume and the agreement in limit with asymptotic steady state solutions. The proposed algorithm has been tested rather extensively and compared in the limit with the available steady state solutions based upon a simplified velocity function without the densification term [16]. Note, no new complexity is introduced in the marching algorithm by the presence of the density term. It is simply a time-dependent function in the velocity term in the integration step. We next proceed to validate the model against sintering data that has been generated internally as well as taken from published work.

4. Experimental procedure

Green samples were slip cast from a dispersed slurry of pure zirconia (zirconia SYP5.2 supplied by Z-Tech Corp., Australia). Green samples were slipcast [34] from slurries containing 30% solids by volume and deflocculated with dispersant Darvan C (Vanderbilt Co., USA). The casts were first dried and then sintered at 1400, 1500 and 1600°C for sintering time up to 24 h in a Lindberg Furnace (Model 51644). During the sintering cycle, furnace was heated at an average rate of 10°C/min to the peak temperature, held for the desired time period and allowed to cool at its natural rate in a closed environment. The bulk densities of the compacts were measured by the Archimedes method using water as the suspending medium. The sintered samples were sectioned and polished with successive diamond grits of 60, 25, 10, 6, 4, 2 and 0.25 μm size and then thermally etched at 100°C below their sintering temperatures for a period of 1 h. The samples were sputter coated with gold-palladium alloy (~ 10 Å thick coating) and examined in a 100 kV scanning electron microscope (Leica Stereoscan 440). The digital images of the micrographs were also obtained for image analysis. Distribution of grains in equivalent area-radius were determined from the digital images with the help of an image analysis software (NIH Image 1.52; distributed by the National Institute of Health, USA). The resulting 2-dimensional discretized distribution (N_A) of grain disks in sectioned area was converted into a 3-dimensional discretized distribution of spherical grains (N_V) in bulk volume by the Johnson-Saltykov method [35]. This procedure amounts to the solution of the following set of linear algebraic equations:

$$\mathbf{A}N_V = N_A \tag{11}$$

where the elements of the coefficient matrix A are defined in terms of discrete size r_i as:

$$A_{ij} = \sqrt{r_j^2 - r_{i-1}^2} - \sqrt{r_j^2 - r_i^2}\ ; \ \text{if}\ j \geqslant i\ \text{else}\ A_{ij} = 0 \tag{12}$$

In order to prevent erratic and inadmissible results in the solution of about 100 simultaneous equations in Eq. (11), the 2-D cumulative size distribution data obtained from image analysis were fitted to the following sigmoidal form:

$$R_{2D}(r, t) = \left(1 + \left(\frac{r}{c}\right)^b\right)^{-e} \tag{13}$$

where b, c and e are the distribution parameters. This function was chosen as it fitted the experimental data for different time-temperature combinations quite well. In some cases, the computed 3-D distribution N_V contained negative values in fine sizes which is not surprising considering the large size of the matrix A to be inverted in Eq. (11).

This problem was overcome by optimizing the following least squares objective function:

$$\text{Minimize}: \ (\mathbf{A}N_V - N_A)^2 \tag{14}$$

with the constraints that all elements of N_V are non-negative. The computed distribution was transformed into cumulative form and fit to a function of the kind given in Eq. (13) to obtain $R(r, t)$ in terms of b, c, and e, the distribution parameters. All comparisons of data with the sintering models were carried out in cumulative rather than frequency domain, in view of the unavoidable presence of errors in grain size measurements, specially in the fine size range, and the uncertainty introduced in 2-D to 3-D transformation.

As mentioned earlier, the initial cumulative larger size distribution $R(r, 0)$ is one of the model inputs. The initial distributions are defined as those which were heated to 1500 or 1600°C and immediately cooled down to the room temperature without any soak. However, for the 1400°C firing schedule, a soaking time of 2 h had to be given in order to obtain samples of sufficient strength for the subsequent polishing operations.

5. Results and discussion

5.1. Model validation from experimental data for sintering of zirconia

The microstructures of the three samples sintered at 1400, 1500 and 1600°C for 2 h is shown in Fig. 1. The microstructure is fairly uniform and homogeneous.

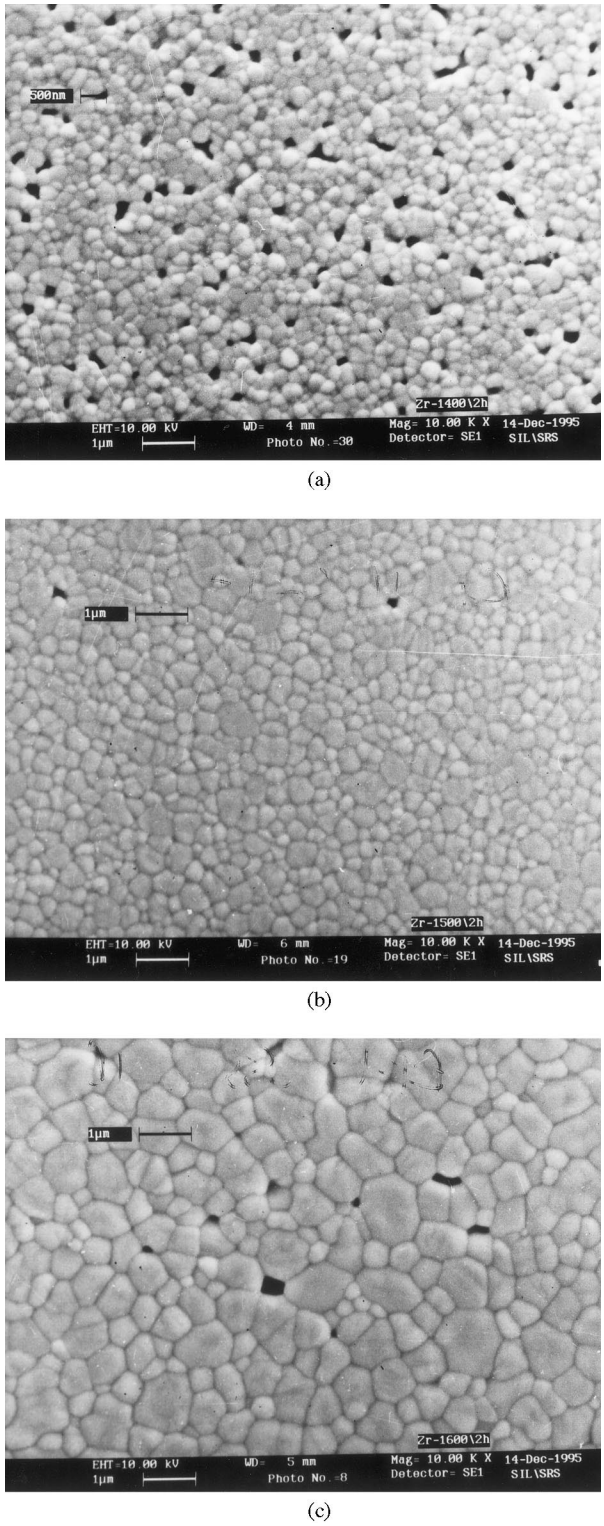

Fig 1. Typical scanning electron micrographs (SEM) showing the microstructure of zirconia specimens sintered at (a) 1400, (b) 1500, (c) 1600°C for 2 h.

The coarsening of microstructure with increasing sintering temperature is also evident from this figure.

The simulation of relative density from the densification model, presented in Part I [24], is compared with

experimentally measured data for zirconia in Fig. 2. It can be seen that the densification model agrees well with the experimental data. The values of the model parameters were found to be $m = 4$ and $k = 18$, 22 and 50 for sintering temperatures of 1400, 1500 and 1600°C, respectively.

The experimentally measured grain size distributions for zirconia samples at 1400, 1500 and 1600°C are plotted for different sintering times in Figs. 3–5. The model predictions for these sintering cycles are also plotted for comparison. The computed values were obtained for a single set of model parameters $n = 2$ and $\alpha = 1$, that gave the best overall fit to the data. The value of C_{GA} refers to the average of 3 values that were used for simulating the grain size distribution corresponding to each time, with a standard deviation of 0.25. It must be recalled that, the experimental data of grain size distribution is generated through the following steps: (a) measurement of areas of two-dimensional grains; (b) determining the radii of circles of equivalent area (c) converting the resulting 2-D distribution to an equivalent 3-D distribution. Considering the number of equivalence assumptions involved, there is considerable source of error in the experimental data. Therefore it is not unreasonable to envisage more than one value of C_G for a given grain growth mechanism operating, for a set of data. Figs. 3 and 4 show a good agreement between the model predictions and experimental grain size distributions at 1400 and 1500°C. However, for the case of 1600°C, the agreement between the experimental data and model is not very good particularly at larger times.

The overall activation energy for grain growth was found to be 533 kJ/mol from the Arrhenius plot shown in Fig. 6. The plot also shows the error bars, which give an indication of the spread in the values of C_G. This value of activation energy for grain growth is close to the value for Zirconia obtained from published data of Yoshizawa and Sakuma [8]. Although, in the above reference, the activation energy was not reported, but it can be

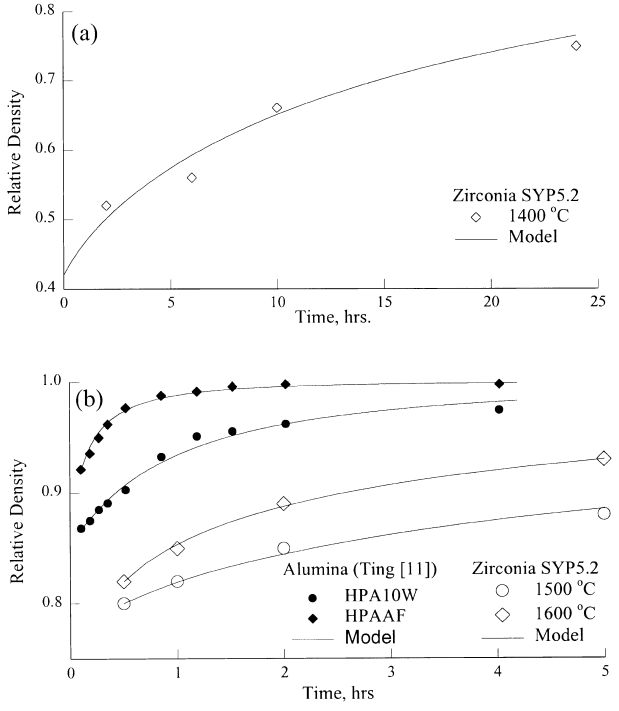

Fig. 2. Comparison of measured and simulated relative density for zirconia SYP 5.2 sintered at (a) 1400, (b) 1500, 1600°C and alumina data (after Ting [11]).

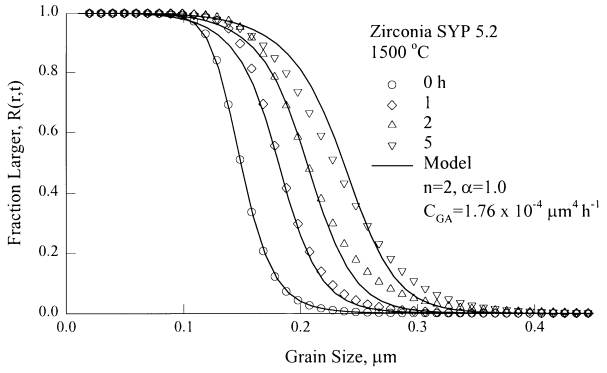

Fig. 4. Comparison of measured and simulated grain size cumulative distributions of zirconia sintered at 1500°C.

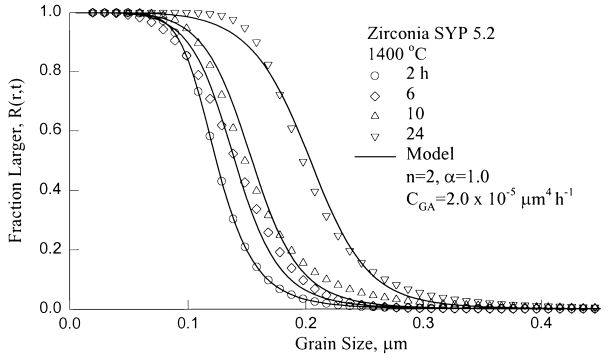

Fig. 3. Comparison of measured and simulated grain size cumulative distributions of zirconia sintered at 1400°C.

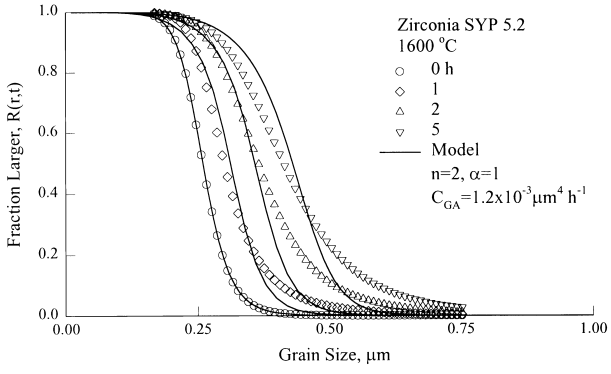

Fig. 5. Comparison of measured and simulated grain size cumulative distributions of zirconia sintered at 1600°C.

readily determined from their data as described below. The grain growth rate as per the model presented in their paper can be written as:

$$\frac{d\overline{d}}{dt} = \frac{K_G}{\overline{d}} \tag{15}$$

where $\overline{d}$ is the mean grain size, and the temperature dependent constant K_G can be expressed as:

$$K_G = M_{gb}\gamma V_m = K_{Go}\exp\left(-\frac{Q_G}{RT}\right) \tag{16}$$

In the Eq. (16), M_{gb} is the grain boundary mobility, V_m is the molar volume and γ is the surface energy. The authors [8] also provides a plot of M_{gb} vs $(1/T)$ along with the values of V_m and γ from which K_G can be computed. The overall activation energy for grain growth (Q_G) was obtained from the plot of $\ln(K_G)$ vs. $(1/T)$ and was found to be 546 kJ/mol, which is comparable to the value (533 kJ/mol) obtained in the present work.

5.2. Model validation from other data (sintering of alumina)

In contrast to the availability of data on pore size evolution, data on the evolution of grain size distribution is rather limited in the literature. Two sets of data, on the sintering of MgO doped alumina published by Ting [11], were selected for validating our model. The median sizes for the materials designated as alumina HPA10W and alumina HPAAF were 0.98 and 0.5 μm, respectively. The alumina compacts were sintered at 1500°C for 10 to 240 min. As corresponding pore size distribution data were not available, for the initial pore size distribution we assumed the same distribution as for the alumina system studied by us earlier in Part I [24]. The model parameters m and k for the pore evolution were then back calculated so as to fit the densification data. The parameter values were $m=6$, $k=1.0\times10^{-13}$ and $m=6$, $k=3.8\times10^{-13}$ for HPA10W and HPAAF respectively. Not surprisingly the densification model showed good agreement [Fig. 2 (b)] with the experimental data. More pertinently, however, quite satisfactory simulation of the grain size spectra could be obtained, as shown in Figs. 7 and 8 for alumina HPA10W and HPAAF, respectively. It must be noted that in spite of the widely different grain size distribution in alumina HPA10W and HPAAF, our model was able to predict the evolution of grain size distribution with time. Due to the non-availability of data for different sintering temperatures, a more complete validation of the model was not possible.

6. Applications — rate controlled sintering

We illustrate the power of our simulation approach with a solution to the common problem of selecting the sintering cycle for a given system. We present here an alternative methodology to the conventional trial and error approach.

In principle, for ceramic systems to be sintered at a certain maximum temperature, there can be an infinite

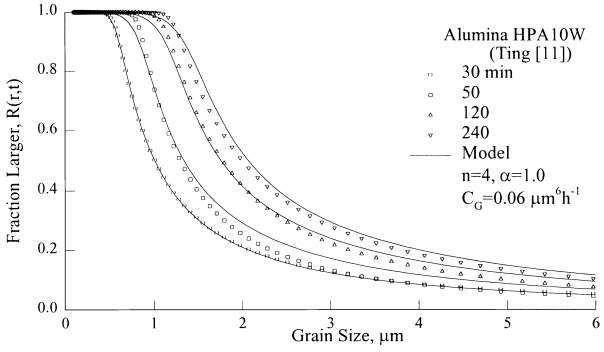

Fig. 7. Comparison of measured (data points) and simulated (solid lines) grain size cumulative distributions of alumina HPA10W sintered at 1500°C. (After Ting [11]).

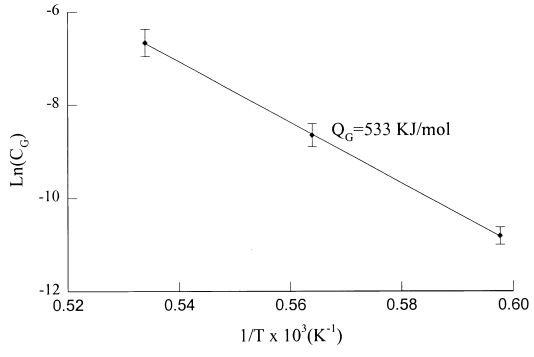

Fig. 6. Arrhenius plot for determination of the overall activation energy of grain growth in zirconia SYP 5.2.

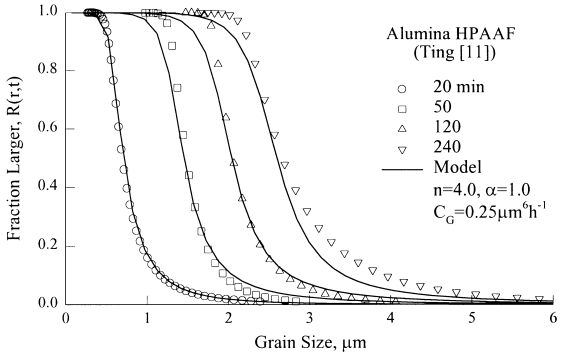

Fig. 8. Comparison of measured (data points) and simulated (solid lines) grain size cumulative distributions of alumina HPAAF sintered at 1500°C. (After Ting [11]).

number of possible cycles to carry out the sintering. However, it has been reported that certain cycles lead to better sintering performance in terms of the densification and microstructure [36–39]. The strategy is referred to as rate controlled sintering. In one example it has been confirmed that using an alternative sintering cycle, the grain growth is minimized without affecting the densification behaviour [40]. We illustrate how our model may be utilized to simulate this case. For the simulation, the parameters of the model, m and $k(T)$ for pore shrinkage, and n and $C_G(T)$ for grain growth, as obtained using the data on sintering of Zirconia, were used. The temperature dependence of the kinetic parameters through the respective activation energies of pore shrinkage and grain growth is given by

$$k = \exp\left(k_0 - \frac{Q_P}{RT}\right)$$

$$C_G = \exp\left(C_{G0} - \frac{Q_G}{RT}\right)$$

The values of the constants used in the simulations are

$m = 4$; $k_0 = 12.2$; $Q_P = 131$ kJ/mol (pore shrinkage)

$n = 2$; $C_{Go} = 27.5$; $Q_G = 533$ kJ/mol (grain growth)

The sintering cycles, Cycle A and B were composed of ramps (R), hold temperatures (T_h) and dwell times (t_d) as given in Table 1. The cycles are shown in Fig. 9 (a). Cycle A is a typical one used conventionally, having a single ramp while Cycle B having four ramps, corresponds to the rate controlled sintering strategy [40]. The sintering simulations were carried out for these two cycles. The predicted sintered density profile, from the simulations are shown in Fig. 9 (b).

We observe that even though the kinetics of densification are altered due to different heating rates of the two cycles, the final extent of densification for the two cases is the same. The grain size distributions for the two cases, at different times (at which the extent of densification is comparable) are compared in Fig. 10. When sintering is carried out using Cycle B, the simulations show that there is reduction in grain growth as compared to that in the case of the conventional cycle.

Thus, in general the model is capable of evaluating the sintering performance of different sintering cycles for any system, thereby enabling rigorous mathematical optimi-

Table 1
Parameters of (time-temperature) sintering cycles employed in simulations

		Ramp, R (°C/min)	T hold, T_h (°C)	t dwell, t_d (h)
Cycle A		12.6	1700	3.75
Cycle B	1	20	1200	0.5
	2	1	1300	0
	3	6	1600	0.5
	4	1.1	1700	0

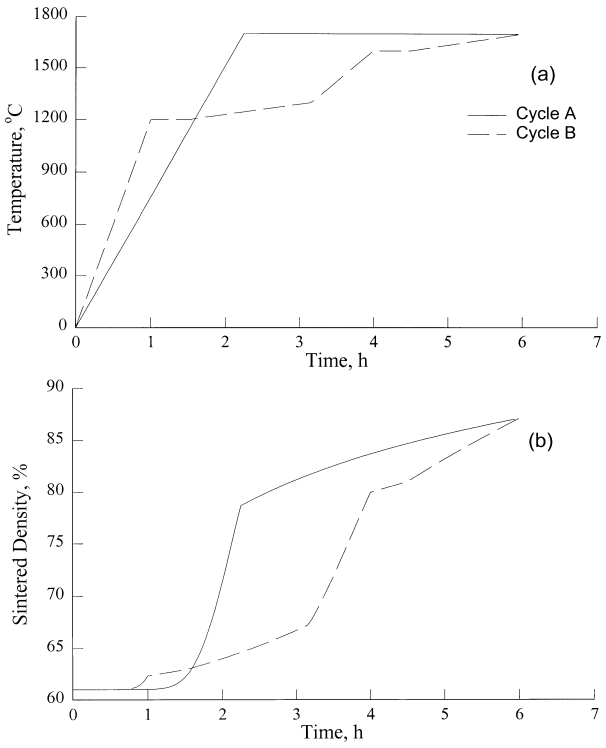

Fig. 9. Sintering simulation — (a) temperature cycles and (b) densification kinetics.

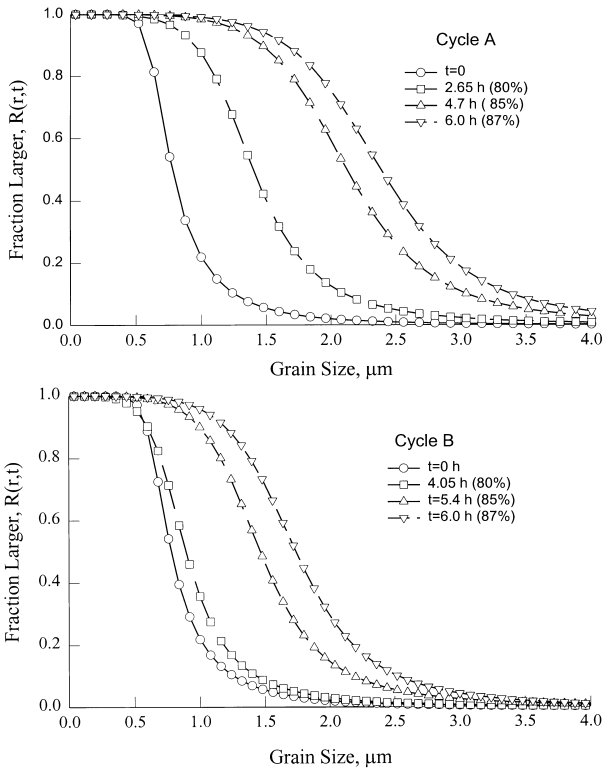

Fig. 10. Evolution of grain size distribution — effect of temperature cycles (sintered densities indicated in brackets).

zation of the sintering cycle for practical sintering systems for a specified objective. Using this approach, one can similarly simulate the effect of various conditions such as the initial size distributions on the kinetics of sintering.

7. Conclusions

It is possible to formulate and, what is equally important, solve a realistic model of sintering kinetics in which the densification and grain growth are coupled together. Because it is based on a formal population balance on particulate entities, the model explicitly reflects the role of the initial size distribution, which most earlier models lack. It is, moreover, capable of providing the complete trajectory of the grain size spectrum. The model proposed by us, is quite general in the sense that any other and, presumably better or more realistic, mechanisms can by readily accommodated in it. Reasonable agreement with zirconia and alumina systems suggests that the model could be useful for control and optimization of the sintering process. In conclusion, we have demonstrated that the evolution of densification and grain size distribution — as a function of sintering temperature/time — can be mathematically described. We have also illustrated how the model can be effectively utilized in designing and evaluating the sintering cycle for a desired sintered product.

Acknowledgements

We gratefully acknowledge support for the work by US-India fund under the auspices of the Department of Science and Technology (DST), India and National Institute of Standards and Technology (NIST), USA. Our sincere thanks to Prof. E.C. Subbarao for his keen interest in this work.

References

[1] M.J. Hoffman, Y.W. Mai, R.H. Dauskardt, J. Ager, R.O. Ritchie, Grain size effects on cyclic fatigue and crack growth behaviour of partially stabilized zirconia, J. Mater. Sci. 20 (1995) 3291–3299.
[2] J.W. Adams, R. Ruh, K.S. Mazdiyasni, Young's modulus, flexural strength, and fracture of yttria-stabilized zirconia versus temperature, J. Am. Ceram. Soc. 80 (1997) 903–908.
[3] H.Y. Lee, W. Reihemann, B.L. Mordike, Grain growth and phase changes during sintering of nanocrystalline zirconia, Mater. Sci. Forum 94/96 2 (1992) 849–854.
[4] L.M. Navarro, P. Reico, P. Duran, Preparation and properties evaluation of zirconia-based/Al_2O_3 composites as electrolytes for solid oxide fuel cell systems: II. Sintering behaviour and microstructural development, J. Mater. Sci. 30 (1995) 1939–1948.
[5] H. Riedel, J. Svoboda, Theoretical study of grain growth in porous solids during sintering, Acta Metall. Mater. 41 (1993) 1929–1936.
[6] J.E. Burke, Grain growth, in: R.M. Fulrath, J.A. Pask (Eds.), Ceramic Microstructures — Their Analysis, Significance and Production, Proceedings of the Third International Materials Symposium, University of California, CA, 13–16 June, 1966, Robert E. Krieger Publishing Co., Hunigton, NY, 1966, pp. 681–700.
[7] G.C. Kuczynski, Science of Sintering 9 (1977) 243–264.
[8] Y. Yoshizawa, T. Sakuma, Evolution of microstructure and grain growth in ZrO_2–Y_2O_3 alloys, ISIJ Int. 29 (1989) 746–752.
[9] P. Feltham, Grain growth in metals, Acta Metall. 5 (1957) 97–105.
[10] F.M.A. Carpey, S.K. Kurtz, A multiple-lognormal model of normal grain growth, in: H. Palmour III, R.F. Davis, T.M. Hare (Eds.), Materials Science Research, vol. 11, Processing of Crystalline Ceramics, Plenum Press, New York, 1977, pp. 217–229.
[11] J.-M. Ting, The Effects of Particle-Size Distribution on Sintering of Alumina, PhD Dissertation, University of Cincinnati, 1991.
[12] J.-M. Ting, R.Y. Lin, Effect of particle-size distribution on sintering. Part I: modelling, J. Mater. Sci. 29 (1994) 1867–1872.
[13] J.-M. Ting, R.Y. Lin, Effect of particle-size distribution on sintering. Part II: sintering of alumina, J. Mater. Sci. 30 (1995) 2382–2389.
[14] K.S. Venkataraman, R.A. DiMilia, Predicting the grain-size distributions in high-density, high purity alumina ceramics, J. Am. Ceram. Soc. 72 (1989) 33–39.
[15] G. Tomandl, Computer calculations of sintering of polycrystalline ceramics, Science of Ceramics 9 (1977) 158–167.
[16] S. Sivakumar, Pradip, P.C. Kapur, S.G. Malghan, A size interval-by-size interval marching algorithm for modelling grain growth in the intermediate stage of sintering, Colloids and Surfaces 133 (1998) 173–182.
[17] G. Venzl, Ostwald ripening of precipitates: I. Numerical solution for the particle size distribution function in closed system, Ber. Bunsenges Phys. Chem. 87 (1983) 318–324.
[18] P.W. Voorhees, M.E. Glicksman, Solution to the multi-particle diffusion problem with applications to Ostwald ripening — II. Computer simulations, Acta Metall. 32 (1984) 2013–2030.
[19] E.A. Barringer, H.K. Bowen, Formation, packing, and sintering of monodisperse TiO_2 powders, J. Am. Ceram. Soc. 65 (1982) C199–C201.
[20] J.P. Smith, G.L. Messing, Sintering of bimodally distributed alumina powders, J. Am. Ceram. Soc. 67 (1984) 238–242.
[21] J.S. Chappell, T.A. Ring, J.D. Birchall, Particle size distribution effects on sintering rates, J. Appl. Phys 60 (1986) 383–391.
[22] T.-S. Yeh, M.D. Sacks, Effect of particle size distribution on the sintering of alumina, J. Am. Ceram. Soc. 71 (1988) C484–C487.
[23] Pradip. Mathematical modelling and simulation of sintering systems, Transactions of PMAI 11 (1984) 62–71.
[24] Manjunath Subbanna, P.C. Kapur, Pradip, S.G. Malghan, Population balance model for solid state sintering: Part I. Pore shrinkage and densification, Ceram. Int. 27 (1) (2001) 57–62.
[25] H.M. Hulburt, S. Katz, Some problems in particle technology: a statistical mechanical formulation, Chem. Eng. Sci. 19 (1964) 555–574.
[26] A.D. Randolph, M.A. Larson, Theory of Particulate Processes, Academic Press, 1971.
[27] H.J. Oel, Crystal growth in ceramic powders, Mater. Sci. Res. 14 (1969) 232–249.
[28] M. Hillert, On the theory of normal and abnormal grain growth, Acta Metall. 13 (1965) 227–238.
[29] M.N. Rahaman, Ceramic processing and sintering, Marcel Dekker, NY, 1995, pp. 445–514.
[30] C. Wagner, Theorie der Alterung von Niederschagen durch Umlosen (Ostwald-Reifung), Z. Electro. Chem. 65 (1961) 581–591.

[31] I.M. Lifshitz, V.V. Slyozov, The kinetics of precipitation from super saturated solid solutions, J. Phys. Chem. Solids 19 (1961) 35–50.
[32] Z. Fang, B.R. Patterson, M.E. Turner, Jr., Influence of particle size distribution on Ostwald ripening, Acta Metall. Mater. 40 (1992) 713–22.
[33] R.T. DeHoff, The analysis of the evolution of particle size distribution during microstructural change, Metall. Trans. 2 (1971) 521–526.
[34] V. Ramakrishnan, S.G.Malghan, Pradip, Yield stess of alumina zirconia suspensions, J. Am. Ceram. Soc. 79 (1996) 2567–2576.
[35] R.T. DeHoff, F.N. Rhines, Quantitative Microscopy, McGraw-Hill, 1968.
[36] Y. Liu, B.R. Patterson, A stereological model of the degree of grain boundary-pore contact during sintering, Metall. Trans. 24A (1993) 1497–1505.
[37] M.L. Huckabee, M.J. Paisley, R.L. Russell, H. Palmour, RCS: taking the mystery out of densification profiles, Ceram. Bull. 73 (9) (1994) 82–86.
[38] T. Ohji, L.C. De Jonghe, Presintering heat treatment, densification and mechanical properties of silicon carbide, J. Amer. Ceram. Soc. 77 (1994) 1685–1687.
[39] M.P. Harmer, R.J. Brook, Fast firing: microstructural benefits, J. Brit. Ceram. Soc. 80 (1981) 147–148.
[40] M.L. Huckabee, T.M. Hare, H. Palmour, Rate controlled sintering as a processing method, in: H. Palmour, R.F. Davis, T.M. Hare (Eds.), Processing of Crystalline Ceramics, Plenum Press, NY, 1978, pp. 205–215.